Iranian Journal of Science and Technology, Transactions of Civil Engineering (2021) 45:1575–1592
https://doi.org/10.1007/s40996-020-00492-9

RESEARCH PAPER

Structural Performance of Steel-Tube Concrete Columns Confined with CFRPs: Numerical and Theoretical Study

Ali Raza[1] · **Babar Ali**[2] · **Anees ur Rehman**[3]

Received: 29 December 2019 / Accepted: 1 October 2020 / Published online: 13 October 2020

Abstract
Fiber-reinforced polymers (FRPs) are being widely used in the structural engineering because of their superior performance over conventional materials such as higher tensile strength, high corrosion resistance, electromagnetic resistance, good durability and light weight. The literature is deficient in the nonlinear finite element analysis (NLFEA) and theoretical predictions of FRP-confined concrete columns. The aim of the present work is to explore the structural performance of steel-tube FRP confined concrete (STC) columns under axial concentric loading. A NLFEA model of STC columns was simulated using ABAQUS which was then, calibrated for different material and geometric models of concrete, steel tube and FRP material using the experimental results from literature. The predictions of proposed NLFEA model were in close agreement with the previous experimental measurements. An extensive parametric study was performed to examine the effects of various parameters of STC columns. Furthermore, a large database of axial strength of 543 confined concrete compression members was developed from the previous researches to propose an empirical model that predicts the ultimate axial strength of STC columns accurately.

Keywords Bearing capacity formula · Steel-tube concrete columns · CFRP-sheets · Nonlinear finite element analysis (NLFEA) · Concrete damaged plasticity (CDP) model · Parametric study

1 Introduction

Fiber-reinforced polymers (FRPs) have superior properties over conventional steel such as low maintenance cost, high corrosion resistance, durability, higher resistance to fire and aesthetic appearance. Stainless steel has favorable mechanical properties to be used in the structures as a competitive material (Gardner et al. 1900). Although the steel tube confinement effectively enhances the concrete strength but, the outward local buckling of the column will decrease the effectiveness of steel tube confinement resulting in the degradation of axial load carrying capacity and ductility of columns (O'Shea and Bridge 2000; Fam et al. 2004). Thus, the additional confinement provided by the fiber-reinforced polymer (FRP) will be useful for the prevention of outward local buckling (Xiao 2004). Due to high stiffness, high corrosion resistance, higher strength, low weight and high durability, composite structures provide many advantages as compared with conventional materials. Thus, they have wide applications in the fields of structural engineering, pressure vessels, aerospace, sports equipment and automotive parts (Van et al. 2003; Shi et al. 2012). Due to lateral confinement, the strength and ductility of the confined concrete are significantly enhanced causing the increase in the use of confined concrete, especially for earthquake resisting structures (Teng et al. 2015).

Many researchers worked on the structural performance of conventional and stainless steel-tube concrete compression members with and without FRP confinements (Lam and Gardner 2008; Liew and Xiong 2009; Han et al. 2014; Perea et al. 2014; Tam et al. 2014; Ding et al. 2015; Liu et al. 2018; Sharif et al. 2019; An and Fehling 2017a; Wang and Liew 2016; An et al. 2019; Xiong et al. 2017; Le et al.

✉ Ali Raza
aliraza@piet.edu.pk

Babar Ali
babar.ali@cuisahiwal.edu.pk

Anees ur Rehman
engr.anees6384@gmail.com

[1] Department of Civil Engineering, Pakistan Institute of Engineering and Technology, Multan 66000, Pakistan

[2] Department of Civil Engineering, COMSATS University Islamabad Sahiwal Campus, Sahiwal 57000, Pakistan

[3] Department of Civil Engineering, University of Engineering and Technology, Taxila 47080, Pakistan

2018; Hoang et al. 2019). From these investigations, it can be observed that the confinements increase the strength and strain ductility of the composite concrete compression members. The structural behavior of the laminated composite concrete structures was superior to either concrete or steel structures because the concrete and confining material give a combined action where the FRP and/or steel tube plays an important role in confining the concrete core material and the concrete core material prevents the local buckling phenomenon. Moreover, the efficiency of concrete-filled stainless steel-tube (CFSST) columns was larger than the efficiency of conventional steel-tube columns. It is also clear from the previous research that the failure mode of the CFSST columns is due to the outwards local buckling causing the degradation in ductility and strength. Therefore, to avoid this local buckling of CFSST columns for further loads, the strengthening needs to be improved by applying FRP laminates around the steel tube. The ductility and axial strength of the concrete core will be significantly improved due to the combined action of steel tube and FRP material. Despite of the structural benefits of CFSST columns, the international standards have not included the design recommendations for such columns. So, there is a need of research in this area to generate the codes and recommendations for the analysis and design of these confined concrete compression members.

It was observed from the literature that most of the previous researches traditionally focused on the experimental investigations to predict the performance of FRP confined concrete members (Richart et al. 1928; Jiang and Teng 2007; Hadi et al. 2016; Huang et al. 2018). Based on the experimental investigations, analytical models for the axial strength and strain of confined concrete columns were proposed (Richart et al. 1928; Mander et al. 1988; Jiang and Teng 2007) which played an important role in predicting the approximate analysis results, but they do not fully explore the fundamental behavior and interaction mechanisms between confinement material and the concrete. To overwhelm the inadequacy of these proposed models for confined concrete, one can move towards the three-dimensional finite element analysis (FEA) with all the deficiencies of analytical models explicitly represented. In comparison with the experiments, FEA simulations can save the cost and time by developing the numerical models which predict the complex damage behavior accurately (Shi et al. 2012). To speed up the simulations and simplify the FEA model, it is essential to consider some assumptions but, it is also important to follow the conditions to be applied in experiments. There should be a balance in model complexity, element types and mesh sizes to enhance the precision of the results and to reduce the time of calculation work. Thus, the numerical methods with the strong background knowledge of FEA are more efficient and convenient tools to be used for the engineering research (Matthews et al. 2000).

Extensive FEA simulations have been performed in the previous research to examine the structural behavior of either concrete-filled steel-tube columns (CFST) or FRP-confined concrete columns (Hu et al. 2011; Ellobody 2013; Hassanein et al. 2013; Tao et al. 2013; Mazzucco et al. 2016; Hoang and Fehlinga 2017; An and Fehling 2016, 2017b; Chau et al. 2019; An et al. 2016). However, none of the researchers developed the FEA model for analyzing the structural behavior of steel-tube FRP confined concrete composite columns. A fiber element model based on the experimental study for the structural performance of CFSST columns was proposed which predicted the numerical and experimental ultimate loads accurately. Moreover, it was concluded that Eurocode 4 and ACI 318 underestimate the axial capacity of CFSST columns significantly (Patel et al. 2014). A nonlinear FEA model of CFSST columns was proposed using ABAQUS (Tao et al. 2011). The FEA prediction in terms of axial load-axial deflection curves and ultimate axial capacity were in a close agreement with the experimental results. Furthermore, by using numerical simulations, the structural performance of carbon steel tube concrete columns was compared with that of CFSST columns. FEA studies on the performance of CFSST columns under concentric loading were performed by Ellobody et al. (2006). The finite element models given by these researchers accurately predicted the structural performance of CFSST columns by taking into account the influence of strain hardening and confinement mechanisms of steel tube.

It can be observed from the literature review that no numerical model for accurately predicting the structural performance of STC compression members has been proposed, as given in the present study. Moreover, no analytical model is available in the literature for the ultimate axial capacity of steel as well as FRP confined concrete compression members. In the present research, first a FEA model was simulated using the software package ABAQUS 6.14. The proposed constitutive FEA model takes into account the influences of steel tube and CFRP sheets strain hardening, high strength materials and confinement mechanisms. Its accuracy was validated against the experiments of STC columns from Liu et al. (2018) by comparing the FEA predictions with the axial load–deflection behavior and cracking patterns. Thereafter, the proposed numerical model was utilized for the extensive parametric study of STC columns to investigate the sensitivity of different critical parameters, material properties and geometric configurations on the structural behavior of columns. Moreover, a large database was developed for the confined concrete strength from the previous researches to propose an analytical model which accurately predicts the axial capacity of STC columns. The present work is

important for the finite element and analytical predictions of axial structural performance of STC columns in a lesser time.

2 Finite Element Simulations

A finite element model (FEM) was proposed using ABAQUS 6.14 for predicting the structural performance of STC columns. The results obtained from the proposed numerical model of STC columns were validated and compared with those obtained from Liu et al. (2018). The numerical model should not be complex which will enhance the analysis time but should be rich enough to capture the essential and critical phenomenon of the structural member. The FEA models of all the STC columns were simulated whose bottom was restrained for all degrees of freedom (DOF), and the top end was kept unrestrained with the applied uniformly distributed axial load on the upper steel plate using displacement control technique. Eight full-scale specimens of STC columns under axial compressive loading were simulated in ABAQUS. The material and geometrical properties of the simulated columns are shown in Table 1. During the FEA simulation, the nonlinear geometric parameter was also included with the specified dissipation energy fraction of 0.0002 to deal with relatively larger displacements. The confined concrete material and the steel plates were modelled as deformable three-dimensional stress, 8-nodded solid brick elements with the hourglass control and reduced integration (C3D8R). The steel tube and CFRP sheets were simulated using the deformable 4-nodded doubly curved shell elements along with the hourglass control and the reduced integration (S4R) having six DOF at each node being capable of predicting the buckling behavior accurately (Sharif et al. 2019). The interaction between the outer concrete surface and the inner steel tube surface was taken as a hard contact in normal direction to avoid the penetration of surfaces into each other and a frictional contact was specified in tangential direction of the member using a frictional coefficient of 0.25 as proposed by Ellobody et al. (2006). Similarly, the connection between the concrete surfaces and the rigid steel plates surfaces was simulated using the hard contact interaction and the frictional contact interaction with a friction coefficient of 0.35 in the normal direction and the tangential direction, respectively (Chang et al. 2013). The surface of concrete core material was taken as master, and the surface of steel plates was assigned as slave surface. The contact between the inner surface of CFRP sheets and the shell elements of steel tube was defined using the constraint "tie" available in the ABAQUS by specifying the interior surface of CFRP sheets and the exterior surface of steel tube as slave surface and master surface, respectively. The node region of steel tube was tied with the surface of steel rigid plates by considering them as a master surface. Figure 1 shows the geometry, steel tube to concrete surface friction interaction, applied loading and meshed elements of the STC columns. The thickness of each CFRP layer was 0.167 mm and the ultimate strength was 3400 MPa. The yield strength and elastic modulus of steel tube were taken as 264.3 MPa and 1.88×10^5 MPa, respectively.

2.1 Simulation of Concrete

There are three models available in ABAQUS, i.e., damaged plasticity model, brittle crack model and smeared crack model, for modelling the nonlinearity of concrete material but concrete damaged plastic (CDP) model is usually preferred (Youssf et al. 2014; Alfarah et al. 2017; Piscesa et al. 2017; Sharif et al. 2019) because it deals broadly with the three-dimensional nonlinear inelastic behavior of concrete including the confinement and damage mechanism, compressive, tensile and plastic properties in the inelastic range. In smeared crack model, cracking is the most important and the compression yielding surface controls the plastic straining whereas in brittle crack model the compressive failure is not important. By using the stress–strain curve of unconfined concrete, we cannot simulate the behavior of FRP-confined concrete accurately (Karabinis and Rousakis

Table 1 Details of geometry and material properties of simulated STC column specimens

Label of column specimen	Diameter of column (mm)	Height of column (mm)	No. of CFRP layers	Thickness of steel tube (mm)	Total thickness of CFRP layers (mm)	Compressive strength of concrete cube (MPa)
L2-C40-D200	200	600	2	2	0.334	57
L4-C40-D200	200	600	4	2	0.668	57
L2-C60-D200	200	600	2	2	0.334	66
L4-C60-D200	200	600	4	2	0.668	66
L2-C40-D260	260	780	2	2	0.334	57
L4-C40-D260	260	780	4	2	0.668	57
L2-C60-D260	260	780	2	2	0.334	66
L4-C60-D260	260	780	4	2	0.668	66

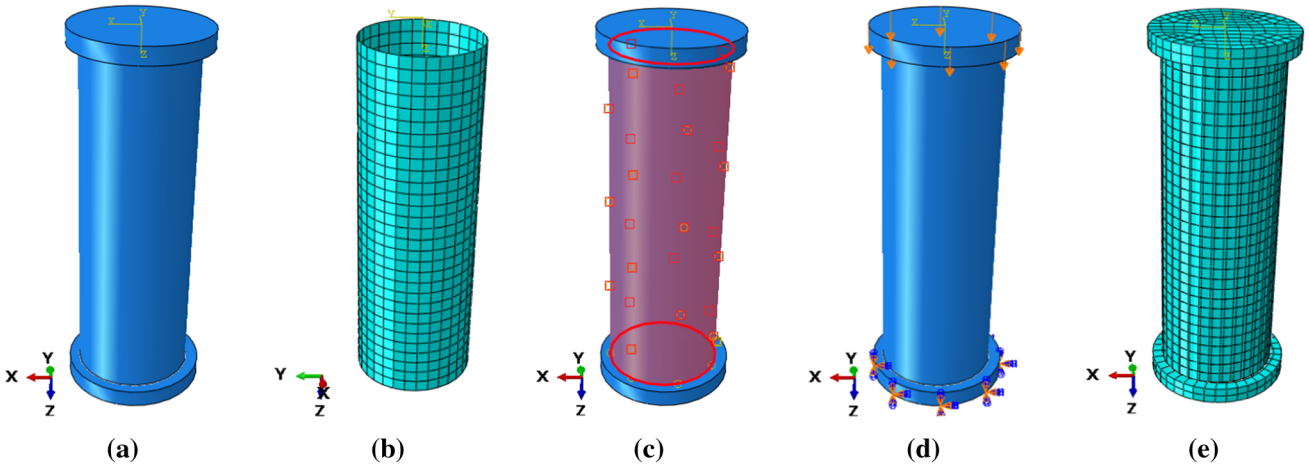

Fig. 1 Finite element simulations **a** geometry, **b** CFRP and steel tube elements, **c** steel tube to concrete surface friction interaction, **d** applied loading, **e** meshed elements of the STC columns

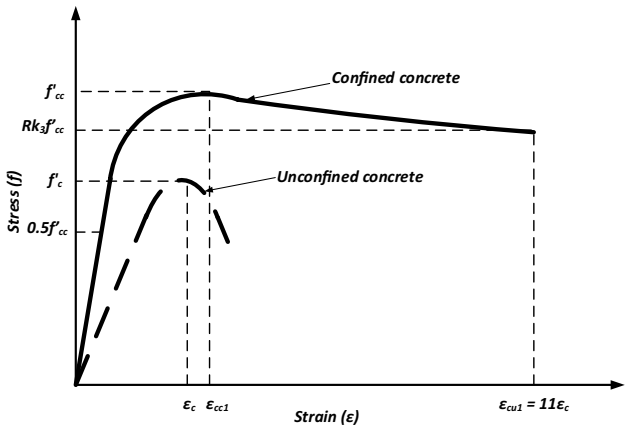

Fig. 2 Axial stress–strain behavior of unconfined and confined concrete

2002; Rousakis et al. 2008; Yu et al. 2010a, b; Hany et al. 2016). Therefore, the concrete was simulated as a confined concrete using the axial stress and strain models of FRP-confined concrete proposed by Mander et al. (1988) after making some modifications in the CDP model. The equivalent stress–strain curve of confined concrete as represented in Fig. 2, was taken from Hu et al. (2003) where f'_{cc} is the axial compressive stress of confined concrete, f'_c is the axial compressive stress of unconfined concrete, ε_c is the compressive strain at. and ε_{cc}. is the axial compressive strain at f'_{cc}. Moreover, r and k_3 are the factors which were calculated using empirical equation available in Hu et al. (2003) and Ellobody et al. (2006).

The linear elastic part of the stress–strain curve can be considered up to 50% of the ultimate strength of confined concrete (Hu et al. 2003; Hassanein 2010) and can be characterized by using two parameters; one is elastic modulus (E_{cc}) and the second is Poisson's ratio. For confined concrete core material, the Poisson's ratio was considered as 0.2 (ASCE 1982) the elastic modulus (E_{cc}) was determined using the equation provided by ACI 318 code as represented by Eq. (1)

$$E_{cc} = 4700\sqrt{f'_{cc}} \tag{1}$$

The nonlinear plastic and damage behavior of confined concrete core was simulated using modified CDP model available in ABAQUS standard. The modified CDP model of concrete is further subdivided into three parts: plastic, tensile and compressive behavior. For the description of the plastic behavior of confined concrete, flow rule, yield surface functions and softening/hardening laws were used. This behavior can be simulated in CDP model using the parameters including the ratio of compressive strengths (f'_{bo}/f'_{co}), the ratio of biaxial to triaxial compressive strengths (K_c), potential eccentricity (ε), viscosity parameter and dilation angle (ψ) of concrete. The values of these parameters were obtained after the calibration. For simulating the compressive behavior, the inelastic strain (ε^{in}) was further increased to define the compression failure at larger strain and peak stress. The compressive behavior consists of compression damage and compression hardening. In cyclic loading, the compression damage variable plays a vital role for the degradation of elastic stiffness of FRP-confined concrete but in monotonic loading the effect of this variable is negligible (Hany et al. 2016). To estimate the strain at ultimate stress (ε_{cc1}) and the ultimate strain ($\varepsilon_{cu1} = 8.7\varepsilon_{cc1}$) of concrete, the relationships represented by Eq. (2) were proposed by Majewski (Majewski 2003).

$$\varepsilon_{cc1} = 0.0014\left[2 - e^{-0.024f'_{cc}} - e^{-0.140f'_{cc}}\right]$$
$$\varepsilon_{cu1} = 0.004 - 0.0011\left[1 - e^{-0.0215f'_{cc}}\right] \quad (2)$$

Similarly, for the modelling of stresses in concrete, Eq. (3) proposed by the Eurocode (CEN 2004) was used.

$$\sigma_{cc} = f'_{cc}\left[\frac{k\left(\frac{\varepsilon_{cu1}}{\varepsilon_{cc1}}\right) - \left(\frac{\varepsilon_{cu1}}{\varepsilon_{cc1}}\right)^2}{1 + [k-2]\left(\frac{\varepsilon_{cu1}}{\varepsilon_{cc1}}\right)}\right], \quad k = 1.05E_{cc}\frac{\varepsilon_{cc1}}{f'_{cc}} \quad (3)$$

where E_{cc} is the modulus of elasticity and f'_{cc} is the ultimate stress of the confined concrete. The tension stiffening model (Nayal and Rasheed 2006) modified by Wahalathantri et al. (2011) was utilized for the numerical simulations of the tensile behavior of confined concrete core material in CDP model as presented in Fig. 3. The ultimate tensile stress (σ_{to}) of concrete was calculated using the equation proposed by Genikomsou and Maria Anna (2015).

$$\sigma_t = 0.33\sqrt{f'_c}\ (\text{MPa}). \quad (4)$$

2.2 Simulation of Steel Tube

The behavior of circular steel tube was simulated using the bilinear elastoplastic model with the concept of von Mises yield criterion as used by Kachlakev et al. (2001), Hassanein (2010), Hassanein et al. (2013), Patel et al. (2017) and Raza et al. (2019) as shown in Fig. 4. The geometry of steel tube material was modelled as 4-nodded shell elements having six DOF at each node with reduced integration (S4R) capturing the buckling behavior with accuracy. According to Rasmussen et al. (2003), the anisotropic behavior of steel is not important when dealing with compression under monotonic axial loading. Therefore, this property of steel tube shell elements was not considered in the present modelling. The elastic part of the bilinear stress–strain behavior of steel tube available in ABQUS was defined by using a Poisson's ratio of 0.3 and an elastic modulus of 188GPa (Liu et al. 2018). The elastic limit was found to be 264.3 MPa. The plastic behavior was defined with a strain hardening ratio of 0.01 (Kachlakev et al. 2001; Raza et al. 2019).

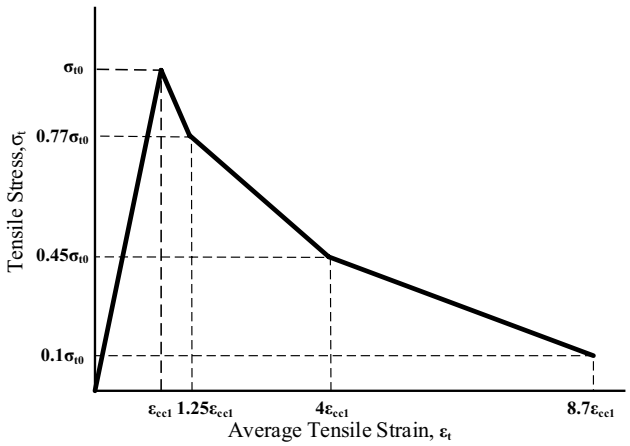

Fig. 3 Tension stiffening model used in present study

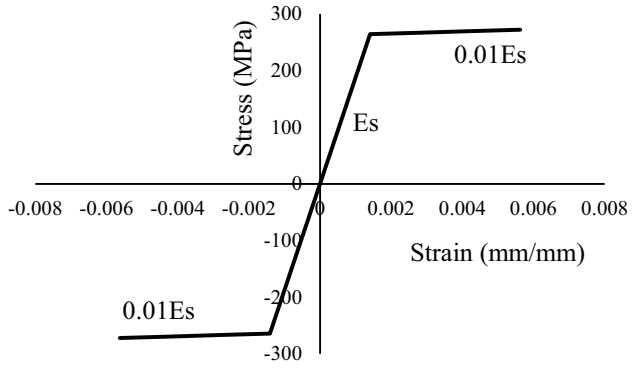

Fig. 4 Bilinear elastoplastic behavior of steel tube

2.3 Simulation of Initial Geometric Imperfections

These are the outward deflections occurring in the thin-walled structural elements whose magnitude is a complex function of geometric and material characteristics and manufacturing and rolling process of the cross sections (Ashraf et al. 2006; Patel et al. 2017). The accurate definition of initial imperfections with proper amplitude and pattern is necessary for a FEA model to capture the behavior of thin-walled structural elements (Sharif et al. 2019). The initial imperfection along the height of column was defined by providing the first positive local buckling mode during the application of axial compressive loading which gives a half-sine wave shape. The FEA model was linked with the required buckling mode shape deflection results after an investigation of elastic buckling. A subroutine naming as "IMPERFECTION" available in ABAQUS software was used to define the initial geometric imperfection with a maximum value of $t/100$ giving the good approach to experimental results, in which "t" is the combined thickness of the confining material (Theofanous et al. 2009). It is important to note that some preliminary analyses were performed in the FEA modelling to find out the proper values of some important parameters of the FEA model.

2.4 Simulation of CFRP Sheets

In laminated composite structures, the internal damage pattern is complicated and difficult to detect (Diaz and Soutis 2000; Díaz and Soutis 2002). In present FEA model, the geometry of CFRP sheet was represented using shell elements (S4R). To define the contact between steel tube and CFRP sheets, a perfect bond was defined by applying "tie" constraint between them. To capture the behavior of CFRP wraps, an accurate definition of laminate strength, elastic and damage evolution is necessary (Sharif et al. 2019). The damage of CFRP sheets can be divided in two categories; one is intralaminar damage occurring within the sheet that can be expressed in fiber tensile and compressive and matrix tensile and compressive failure modes, and second is the delamination or interlaminar damage occurring between the neighboring layers (Shi et al. 2012). The damage of composites is highly dependent on the misalignment of the fibers and the shear behavior of resin. The transverse cracks occurring due to tensile loading can cause the matrix or fiber interfacial damage. From the experiments, it has been observed that the shear matrix damage dominates the matrix compression damage by creating a fracture plane along the direction of through-thickness of the fiber (Anderson 1995).

The elastic behavior of CFRP sheets was simulated using the material type as "LAMINA" in which the elastic modulus in hoop direction E_1 was taken from the manufacturer with a value of 235 GPa (Liu et al. 2018), and small percentages of elastic behavior in the direction of fiber were assigned to E_2, G_{12}, G_{13} and G_{23} (Hany et al. 2016; Sharif et al. 2019). The value of Poisson's ratio was taken as 0.3. The failure stress in suboption of elastic behavior was defined by using a tensile stress of 3400 MPa provided by the manufacturer (Liu et al. 2018) in fiber direction while small percentage values of tensile stress in fibers' direction were used for compressive stresses in fiber and transverse directions for matching the FEA predictions closely with the experimental outputs as shown in Table 2.

Hashin damage criterion (Hashin and Rotem 1973; Hashin 1980) was used in the present research to model all the modes of failure of CFRP laminates consisting of strength and damage behavior as this model accurately predicts the fiber and matrix tensile and compressive damage initiation (Shi et al. 2012). The strength properties of CFRP laminates were defined by using the manufacturers' provided tensile strength in fibers' direction and some assumed as small values of that strength in perpendicular direction as reported in Hany et al. (2016) to match the FEA predictions with the experiments. After the initiation of damage criterion, degradation of the stiffness coefficients will occur upon the application of further loading. The evolution of damage parameters of FRP material employs the energy release rates according to four damage modes (Barbero et al. 2013). The damage evolution parameters were taken according to Shi et al. (2012). Different parameters used to describe the Hashin damage model for CFRP laminates are presented in Table 3.

Table 2 Elastic behavior of CFRP

Property	Value
Elastic modulus in fiber' direction, E_1 (GPa)	235
Elastic modulus in transverse direction, E_2 (GPa)	10.68
Longitudinal-transverse Poisson's ratio, Nu_{12}	0.3
Shear moduli, G_{12}, G_{13}, G_{23} (MPa)	5405

2.5 Validation of Proposed NLFEA Model

A STC column (L2-C40-D200) from (Liu et al. 2018) was taken as a control specimen for calibration and validation purposes. The FEA model of L2-C40-D200 was calibrated

Table 3 Strength and damage variables of Hashin model

Strength properties	
Tensile strength in normal dir. of fiber (MPa)	3400
Compressive strength in normal dir. of fiber (MPa)	11.34
Tensile strength in transverse dir. of fiber (MPa)	11.34
Compressive strength in transverse dir. of fiber (MPa)	11.34
Shear strength in normal dir. of fiber (MPa)	11.34
Shear strength in transverse dir. of fiber (MPa)	11.34
Damage properties	
Fracture tensile energy in fibers' dir. (mJ/mm^2)	92
Fracture tensile energy in transverse dir. (mJ/mm^2)	1.1
Fracture compressive energy in fibers' dir. (mJ/mm^2)	1.1
Fracture compressive energy in transverse dir. (mJ/mm^2)	0.2

for different boundary conditions, geometric properties and material properties in order to obtain the accurate results as compared with that of experiments of the axial capacity, load–deflection behavior and failure patterns. The definition of the plastic region of concrete behavior requires the description of flow rule, hardening and softening laws and shape function of yielding surface. The dilation angle of concrete, which is a material parameter, belongs to the nonassociated flow rule. The CDP model for the accurate simulations of the plastic behavior of concrete uses the flow potential function which is basically defined by Drucker–Prager hyperbolic function. Wu et al. (2006) and Voyiadjis and Taqieddin (2009) suggested that the value of ψ should be in between 31° and 42°. Therefore, this parameter of the plastic behavior of concrete was calibrated using the load–deflection curve of control specimen (L2-C40-D200) for the values of 30°, 33°, 36°, 39°, 42° and 45° in order to achieve the accurate predictions. The best approximation was achieved using 30° for ψ which was selected for the control model (L2-C40-D200) as shown in Fig. 5a. It was examined that the effect of ψ was significant in the post-buckling behavior of concrete but was negligible in elastic behavior.

The sensitivity of load–deflection performance of the control specimen due to viscosity parameter of concrete was shown in Fig. 5b. For the better convergence of FEA results, a smaller value should be used for the viscosity parameter. The time increment size influences this parameter and its value should always be approximately to 15% of time increment size for achieving the good results as compared with experimental results (Lee and Fenves 1998). The ultimate axial strength of control specimen was increased up to 27% when the viscosity parameter was increased from 0.0009 to 0.009. The selected value of this parameter was 0.005 because of the good results at this value in comparison with the experimental load–deflection response. The study of the effect of K_c on the load–deflection behavior predicted the value of K_c as 0.667 as represented in Fig. 5c. Using a relatively smaller value of K_c (0.5) does not allows the concrete for degradation and

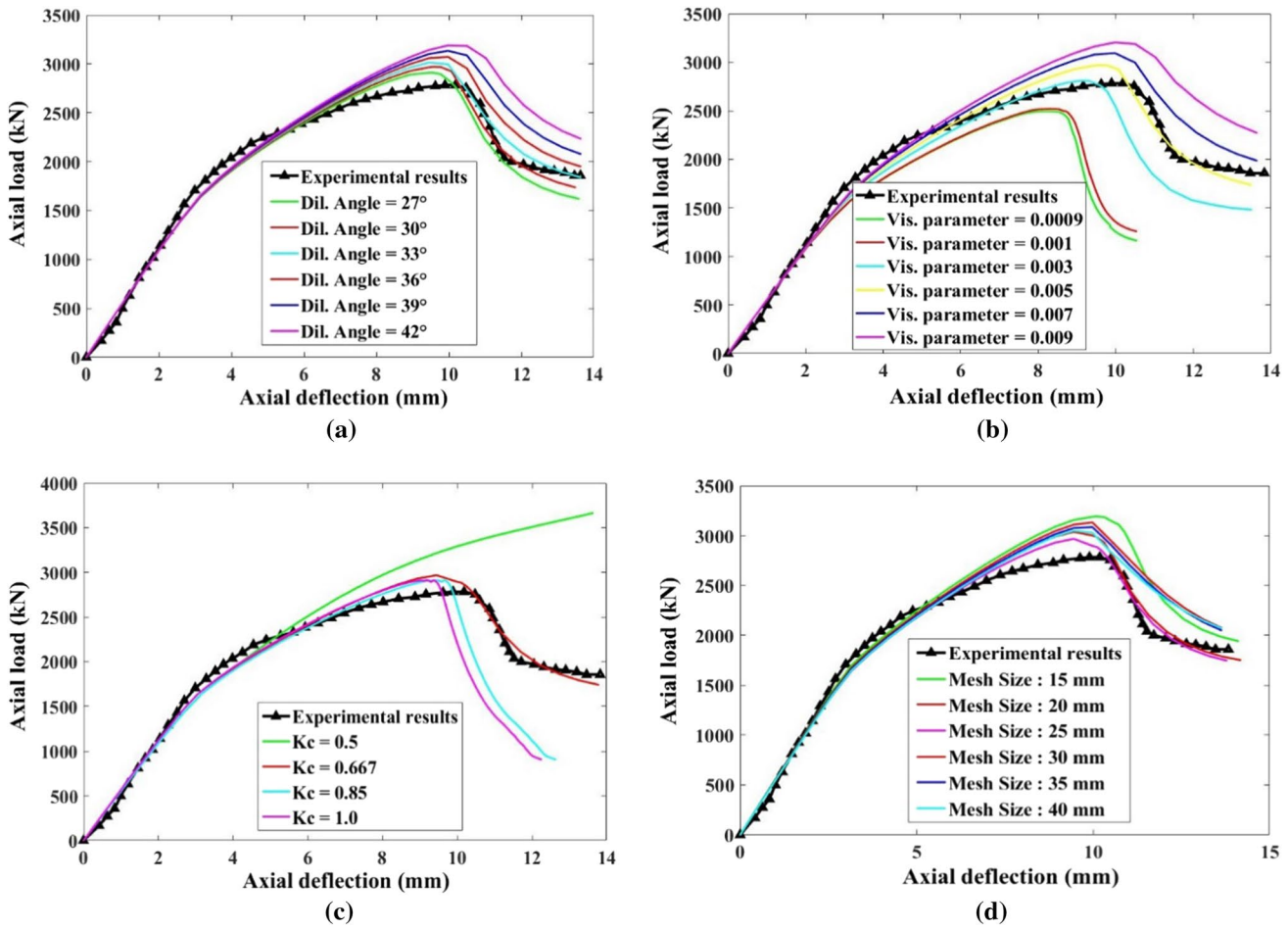

Fig. 5 Sensitivity of different parameters on load–deflection performance of control model, **a** dilation angle, **b** viscosity parameter, **c** shape factor, **d** mesh size of elements

using a larger value (1.0) allows the control specimen to fail at smaller load and smaller deflection. The value of 0.667 gave the best approximation with the experimental results and hence, was selected.

Element sizes of 15, 20, 25, 30, 35 and 40 mm were studied to determine the mesh size giving the best approximation to the experimental curve of load–deflection of STC columns. At 15 mm mesh size, the ultimate load and corresponding axial deflection were 108% and 107% than that of 25 mm mesh size. A close agreement between the FEA and the experimental predictions of load–deflection behavior was obtained using the elements of 25 mm size which was selected for the further analysis of the STC columns and their parametric study. The effect of different mesh sizes is represented in Fig. 5d.

The element library of ABAQUS consists of various types of 3D stress and shell elements. The 3D concrete material was calibrated for triangular elements (C3D15H and C3D6H), hexahedral elements (C3D20R and C3D8R) and tetrahedral elements (C3D10H and C3D4H). A close relation between FEA predictions and that of experiments was obtained using 8-noded brick elements (C3D8R) of concrete which is also reported by the literature (Hany et al. 2016; Najafgholipour et al. 2017). The calibration for elements types of steel tube and CFRP sheets was conducted using the quadrilateral and triangular shell elements. The quadrilateral elements consist of linear and quadratic conventional shell elements (doubly curved) with reduced integration for large strains (S4R and S8R) and the triangular elements consist of linear and quadratic shell elements (S3R and STRI65) which were used in the current research for the convergence purpose of control model as represented in Fig. 6. A standard 4-noded shell element (doubly curved) with hourglass control and reduced integration presented the close agreement among experimental and FEA predicted results of the load–deflection behavior of control specimen (L2-C40-D200). Generally, it was concluded that the sensitivity of varying the elements types on the load–deflection performance was not significant.

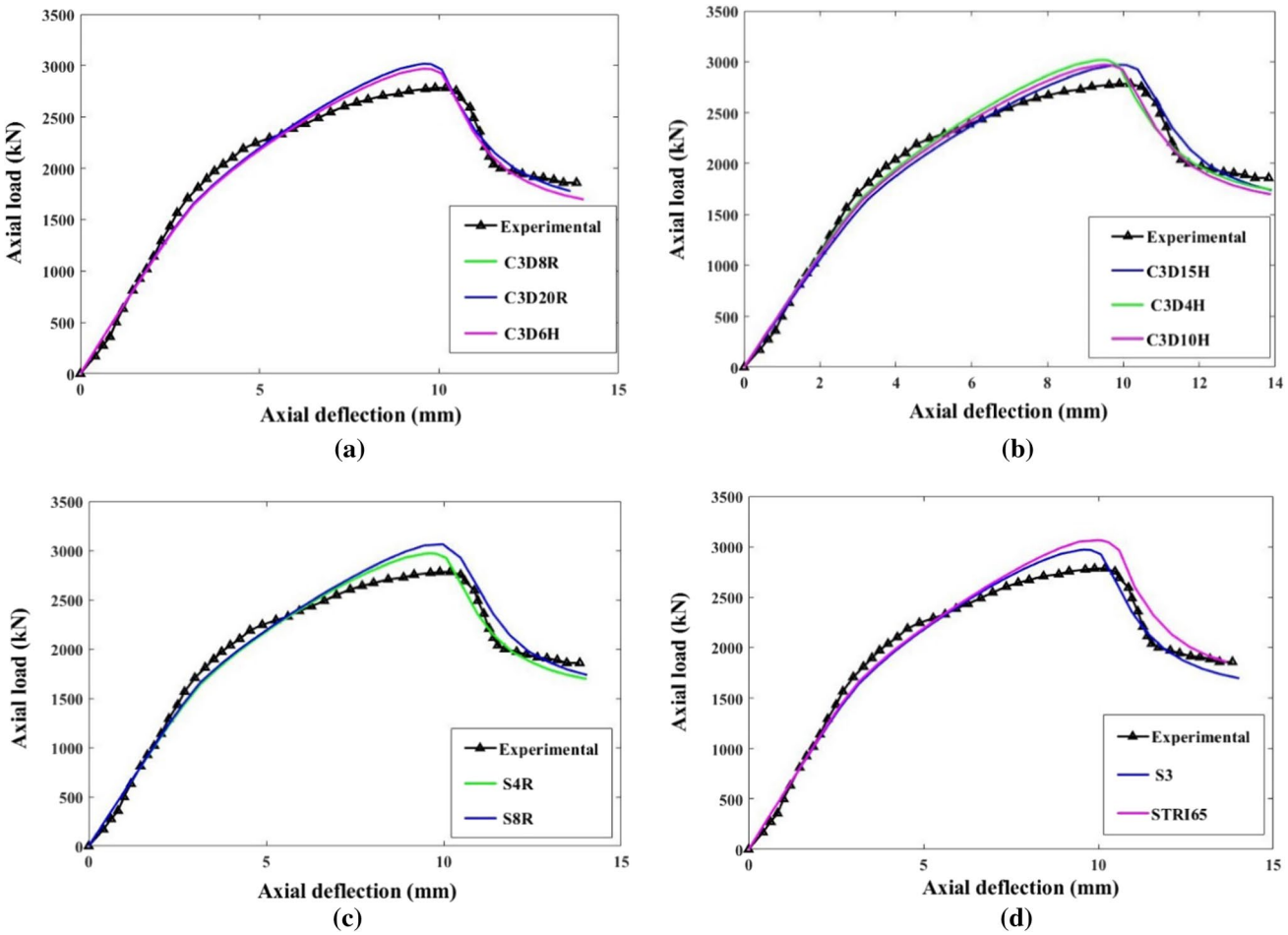

Fig. 6 Load–deflection behavior of control finite element model for different element types, **a** linear plain stress, **b** quadratic plain stress, **c** quadrilateral elements of steel tube and CFRP shell elements, **d** triangular elements of steel tube and CFRP shell elements

3 Discussion of Results

3.1 Load–Deflection Response

The structural response of STC columns in terms of axial load–deflection curves was represented in Fig. 7. The parameters of the plastic behavior of concrete in the modified CDP model were taken as same for all the specimens after calibration. It can be observed from Fig. 7 that the FEA model captured the experimental results accurately in the elastic as well as inelastic behavior of columns. The maximum percentage difference between the experimental and numerical results of the ultimate axial capacity was observed for the specimen having compressive strength of 40 MPa, 4 CFRP layers with a concrete core diameter of 260 mm (L4-C40-D260) which was 8.91%. It was also noticed that

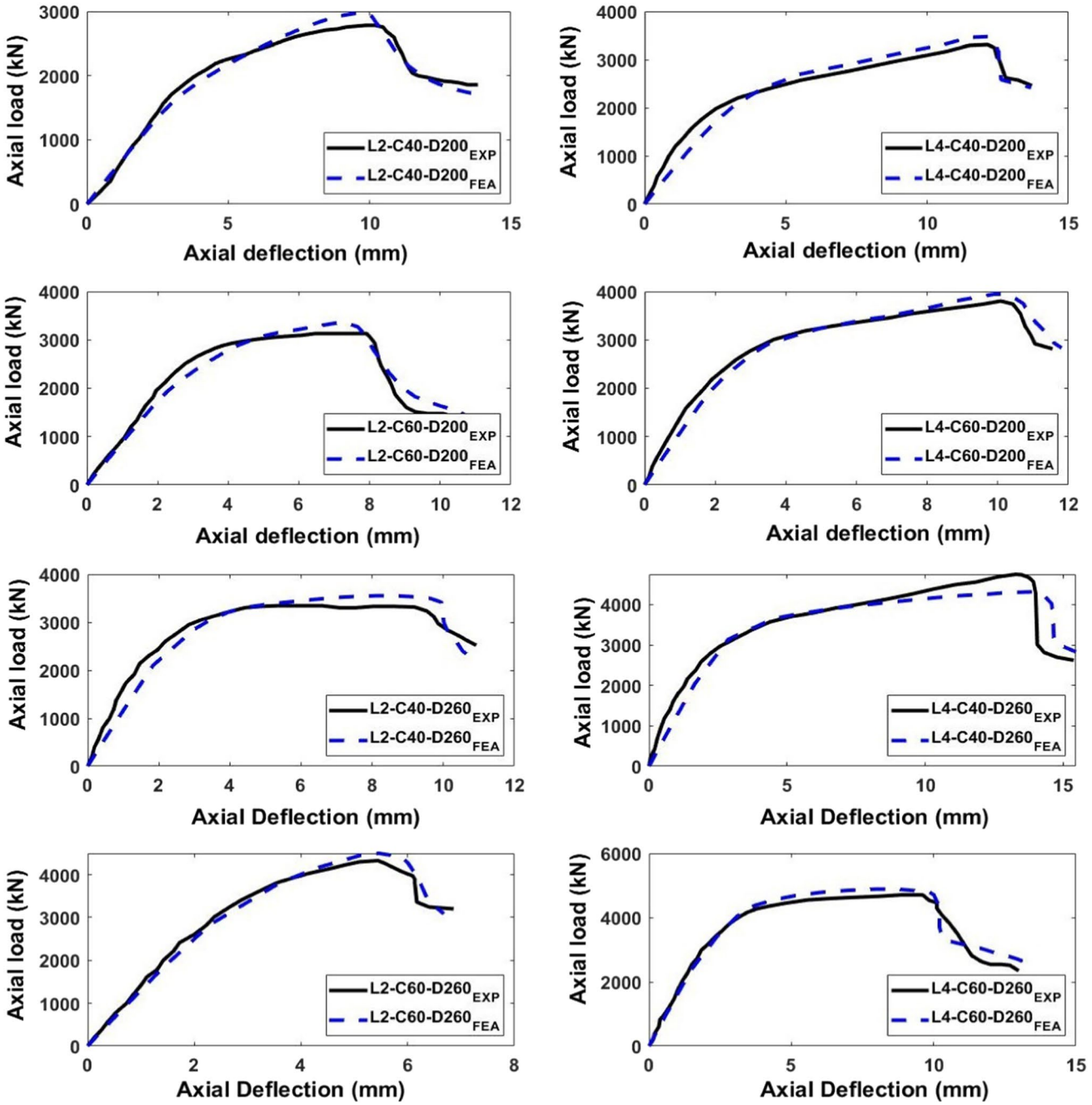

Fig. 7 Experiments and FEA results of load–deflection response of steel-tube CFRP confined concrete columns

the experimental results were stiffer that the predictions of the FEA model in elastic region but, in inelastic region, there was a close agreement between them. Similarly, the maximum percentage difference for the deflection at ultimate load was observed for the specimen L2-C40-D260 with a value of 7.85%. The average percentage discrepancies in the ultimate strength and the deflection at that strength of the STC columns were 5.76% and 2.86%, respectively. These discrepancies may be ascribed to the small imprecisions resulting from the differences between the actual testing conditions such as boundary conditions, initial geometric imperfections, strength of concrete material, strength of steel material, manufacturing faults, accuracy of the testing instruments and the conditions assumed in the FEA modelling. The difference may also be attributed to definition of the damage evolution parameters of CFRP material and the friction coefficients assumed for the contact property between the steel and concrete materials.

3.2 Effect of CFRP Layers

Either two or four layers of CFRP sheets were studied numerically in the present research. The effect of CFRP layers was represented in Fig. 8. It was observed that the specimens with 200 mm diameter having a concrete strength of 40 MPa (C40-D200) showed a percentage increase of 18.99% in the ultimate capacity and 22.65% in the deflection at ultimate capacity due to increase of CFRP layers from two to four. Similarly, the specimens with 200 mm diameter with 60 MPa concrete strength (C60-D200) showed 21.54% and 37.33%, the specimens with 260 mm diameter with 40 MPa concrete strength (C40-D260) showed 42% and 67.87% and the specimens with 260 mm diameter with 60 MPa concrete strength (C60-D260) showed 8.58% and 71.69% increase in the ultimate axial loading capacity and corresponding deflection, respectively. Thus, the maximum increase in the axial loading capacity and ductility was observed for the specimens C40-D260 and C60-D260, respectively. As concerned with the FEA results, the maximum increase in the axial loading capacity and ductility was observed for the specimens C40-D260. The average percentage error in the percentage increase of ultimate axial load and corresponding deflection due to increase of CFRP layers from two to four was 33.22% and 13.85%, respectively, when FEA results were compared with that of the experiments.

These minor discrepancies between the experimental and FEA results may be ascribed to the supposition of a perfect bond between the steel tube and CFRP sheets in the FEA. Moreover, it is very difficult to accurately apply the actual experimental testing conditions in the FEM. However, the proposed FEA model accurately traced the increase in ultimate capacity and corresponding deflection due to increase of CFRP layers.

3.3 Effect of Unconfined Concrete Strength

Two different values of unconfined compressive strengths of concrete (40 MPa and 60 MPa) were investigated to observe their effect on the load–deflection behavior of STC columns. The effect of increasing the unconfined compressive strength of concrete was significant on the ultimate axial capacity. The increase in the axial capacity was 12.39% for the columns with two CFRP layers and 200 mm diameter, 14.8% for the columns with four CFRP layers and 200 mm diameter and 29.86% for the specimens with two CFRP layers and 260 mm diameter. The increase in the capacity was negligible while increasing the concrete strength from 40 to 60 MPa for the specimens with four CFRP layers and 260 mm diameter. It was examined that the deflection at ultimate axial load was reduced by increasing the concrete

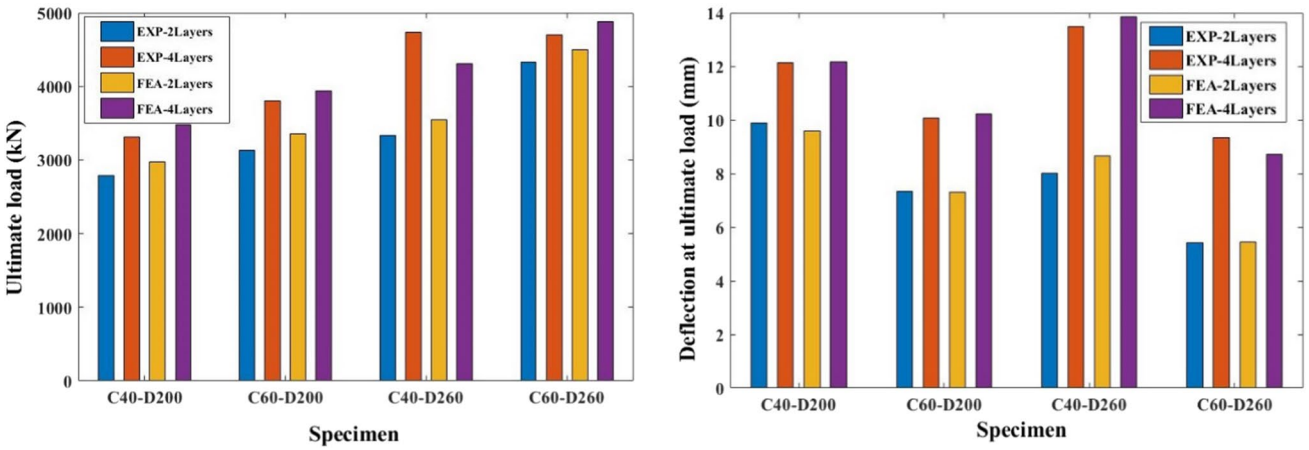

Fig. 8 Effect of CFRP layers on the axial-deflection at ultimate capacity of STC columns

strength. The maximum percentage decrease in the deflection was occurred for the specimens with 260 mm diameter and four CFRP layers with a value of 30.71%. The FEA model predicted the effect of increasing the strength of concrete with minor errors. The average percentage error in the percentage increase of ultimate capacity of columns due to increase of unconfined concrete strength was 21% and that of deflection at ultimate capacity was 11.15%. Thus, the proposed numerical model can acutely capture the behavior of STC columns due to increase of unconfined concrete strength.

3.4 Failure Modes

During the early stages of loading, there was observed a linear trend between the axial loading and deflection of STC columns but after the yielding of steel tube, the axial loading was linearly increased creating the second linear part of the curve. Then, the axial loading reached to the ultimate capacity of the members along with the rupture of CFRP-wraps causing the rapid drop in the axial capacity. It was observed from the finite element simulations of 8 STC specimens that all the columns presented combined shear and crush failure modes as shown in Fig. 9 for the two specimens L2-C40-D200 and L2-C60-D200. The crack patterns of FEA models were visualized by maximum positive plastic strain (PE, principal) because the direction of cracks is always normal to the PE, principal in concrete material which accurately represents the cracks patterns (Genikomsou and Maria Anna 2015; Raza et al. 2019, 2020; Raza and Khan 2020).

In conclusion, crush failure was more dominant for the STC columns with lower strength of unconfined concrete and more layers of CFRP sheets. Conversely, the shear failure was more dominant for the STC columns with higher strength of unconfined concrete and a smaller number of CFRP sheets.

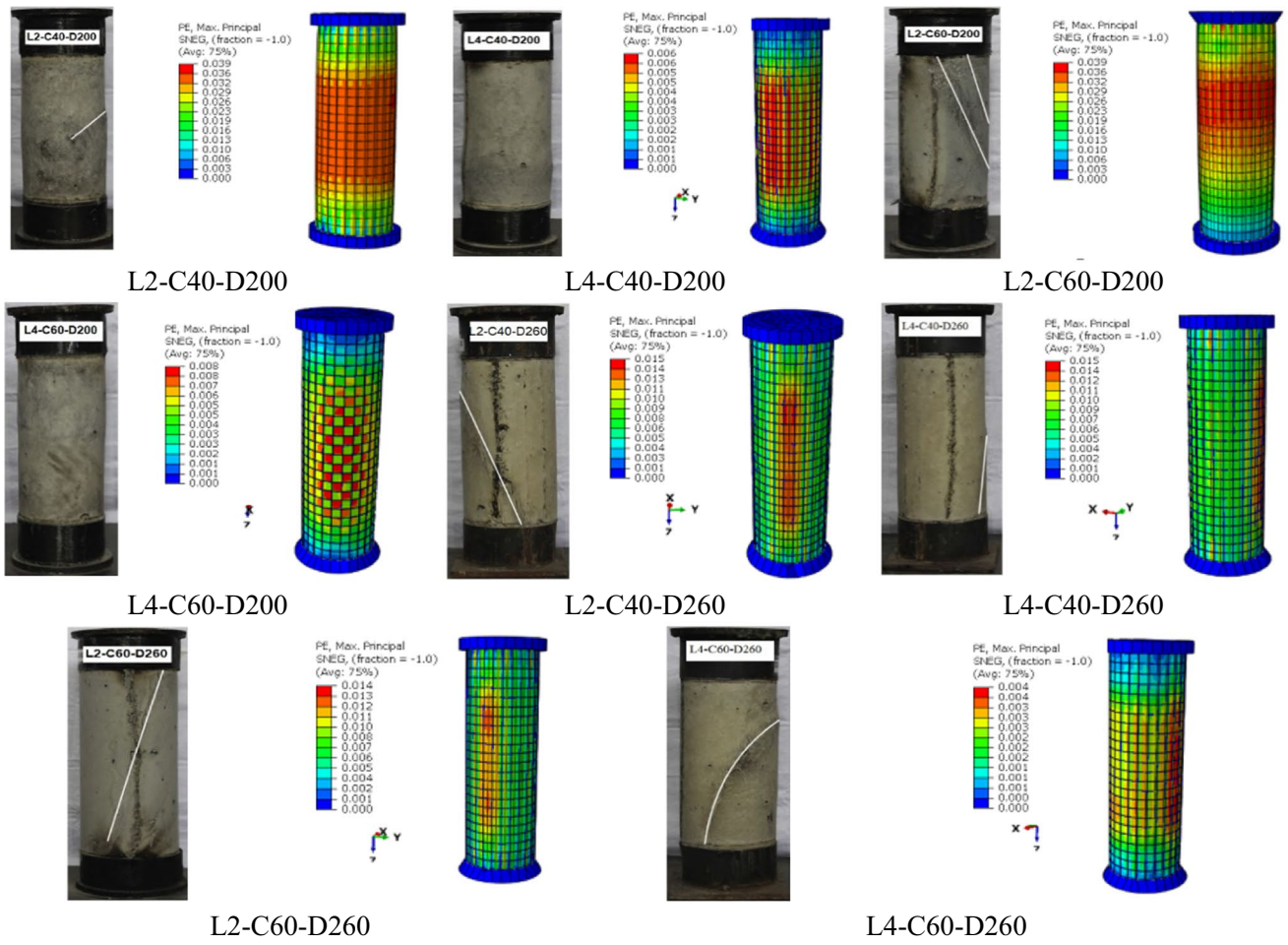

Fig. 9 Experimental and FEA cracks patterns of **a**, **b** L2-C40-D200, **c**, **d** L4-C40-D200, respectively

4 Parametric Study

After validating the selected FEA model through experimental results of 8 STC columns, 216 models were analyzed to examine the effect of CFRP layers, unconfined concrete strength (f'_{co}), thickness of steel tube (t_s) and diameter of concrete core (D) on the load–deflection performance. Different values of the parameters for the parametric study were given in Table 4. The height of all the specimens was 600 mm. The yielding strength and elastic modulus of steel tube and the ultimate strength CFRP sheets were taken according to Liu et al. (2018).

4.1 Effect of CFRP Layers

Six levels of CFRP layers were studied: 0, 1, 2, 3, 4 and 5 layers, respectively. Throughout the parametric study, the thickness of each CFRP layer was taken as 0.167 mm. It was observed that when CFRP layers were increased from 0 to 5 at contact t_s of 2 mm and constant D of 200 mm of the column with the increase of f'_{co} from 15 to 65 MPa, the percentage increase in the capacity of STC column was 179.01%. Similarly, with the increase of CFRP layers from 0 to 5 while increasing the t_s from 0.5 to 3 mm at constant f'_{co} of 25 MPa and constant D of 200 mm, the percentage increases in the capacity was 64.02%. Moreover, the effect of increase of CFRP layers was 1282.69% with the increase of D from 100 to 350 mm at constant f'_{co} of 25 MPa and t_s of 2 mm. The sensitivity of CFRP layers on the ultimate axial capacity of STC columns with the increase of f'_{co}, t_s and D was presented in three-dimensional Fig. 10a–c. It can be monitored that the effect of increase of number of CFRP layers along with the increase of diameter was more dominant with the percentage increase of 1282.69% in axial capacity.

4.2 Effect of Unconfined Concrete Strength (f'_{co})

The effect of variation of f'_{co} on the ultimate axial capacity was represented in Fig. 10a, d, e. The plastic parameters of concrete were kept same for the parametric study, but the compressive and tensile behavior was changed accordingly.

Table 4 Variables for finite elements parameter study

Parameters	Constant values	Varying values
CFRP layers	2.0	0, 1, 2, 3, 4, 5
f'_{co}	25	15 MPa, 25 MPa, 35 MPa, 45 MPa, 55 MPa, 65 MPa
t_s	2.0	0.5 mm, 1 mm, 1.5 mm, 2 mm, 2.5 mm, 3 mm
D	200	100 mm, 150 mm, 200 mm, 250 mm, 300 mm, 350 mm

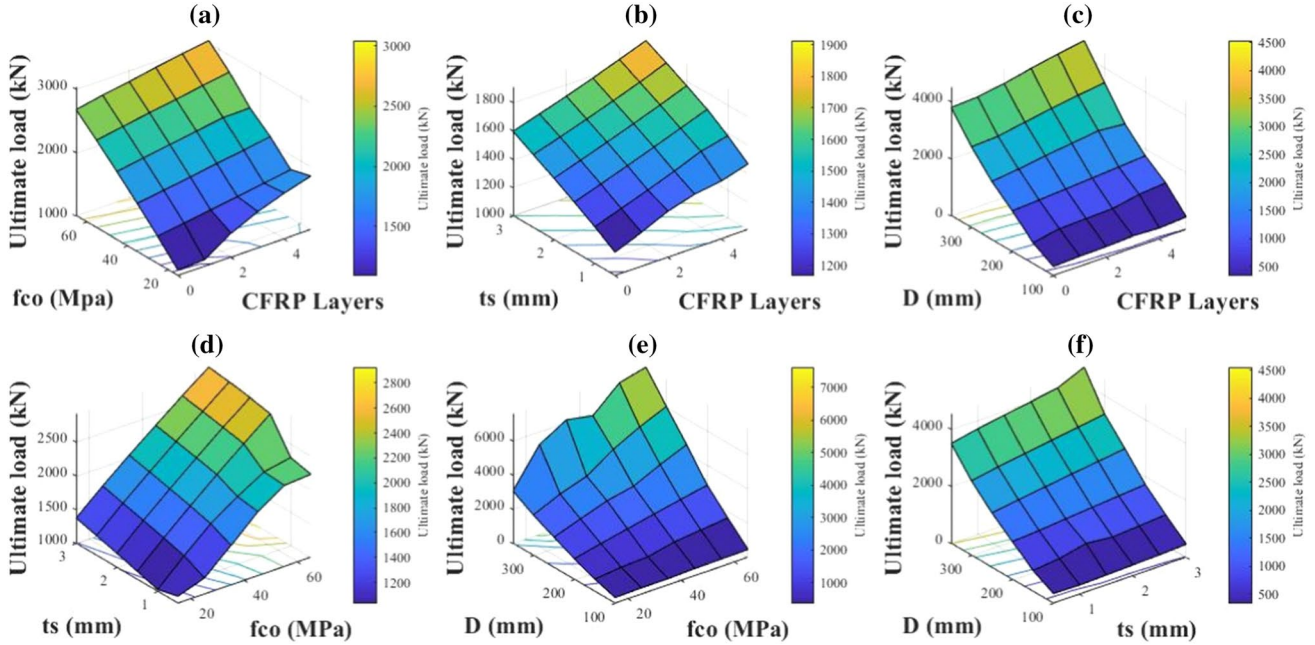

Fig. 10 Effect of CFRP layers, concrete strength, steel tube thickness and diameter of columns on the ultimate axial capacity of STC columns

It was observed that with the increase of f'_{co} from 15 to 65 MPa along with the increase of CFRP layers from 0 to 5 at constant t_s of 2 mm and constant D of 200 mm, the percentage increase of 179.01% was occurred for axial capacity of STC columns. When f'_{co} was increased with the increase of t_s from 0.5 to 3 mm, the percentage increase of 222.23% was observed for ultimate capacity. Similarly, the effect of increase of f'_{co} was 2157.44% due to increase of diameter of columns for axial capacity.

4.3 Effect of Steel Tube Thickness (t_s)

Various studied values for the thickness of steel tube were 0.5 mm, 1 mm, 1.5 mm, 2 mm, 2.5 mm, and 3 mm to explore their effect on the capacity of STC columns. By increasing the t_s from 0.5 to 3 mm along with the increase of number of CFRP layers from 0 to 5 layers, the percentage increase of 64.02% and 34.74% occurred in ultimate capacity. Similarly, with the increase of t_s from 0.5 to 3 mm, the percentage increase of 1192.63% for load was occurred with the incrementation of diameter from 100 to 350 mm at constant f'_{co} of 25 MPa and two CFRP layers as shown in Fig. 10.

4.4 Effect of Diameter of Column (D)

The diameter of columns (D) was studied up to 6 levels: 100 mm, 159 mm, 200 mm, 250 mm, 300 mm, and 350 mm to determine its sensitivity on the load–deflection behavior of STC columns. The effect of variation of D was presented in Fig. 10c, e, f. It was observed that the effect of increase on diameter of column remained more significant for the increase of ultimate capacity of columns. The percentage increases of 1282.69%, 2157.44% and 1192.63% were observed for ultimate capacity while increasing the diameter up to 350 mm with the increase of number of CFRP layers from 0 to 5 layers, f'_{co} from 15 to 65 MPa and t_s from 0.5 to 3 mm, respectively. Hence, it can be deduced from the extensive parametric study that the effect of increasing the CFRP layers, f'_{co}, t_s and D of the STC columns was significant for the increment in their capacity with the dominant effect of increase of D.

5 Proposed Capacity Equation

5.1 Data Generation

It was concluded from the literature review that no analytical model was proposed for predicting the axial strength of STC columns except (Sharif et al. 2019) who derived the analytical model from FEA parametric study only, but in the current research, the analytical model was proposed based on the large experimental database giving more accurate results of the ultimate axial capacity of STC columns. A large database of confined concrete strength was developed from the previous researches and evaluated based on the previously proposed strength models to remove the error giving data points which cause the saturation of RMSE index. After removing the data points giving error more than 20%, 543 sample points were left which were used for the general regression analysis to propose the confined concrete strength model. The statistical information of the developed database is given in Table 5.

5.2 Assessment of Empirical Models

The analytical model to predict of axial capacity of STC columns consists of two parts: one is due to confinement stress and the second is due to ultimate capacity of steel tube. For the first part of the analytical capacity model, the strength models of confined concrete given by Lam and Teng (2003), Toutanji (1999), Teng et al.(2009), Saafi et al.(1999), Miyauchi et al. (1997) and Matthys et al. (2005) were evaluated using some statistical parameters such as root-mean-square error (RMSE), coefficient of determination (R^2) and the sum of squared errors (SSE) on the developed database to propose a general form of the analytical model. The performance of Lam and Teng (2003) model remained good with RMSE = 0.244 and R^2 = 0.903. Thus, the general form of the confined concrete strength equation was adopted from this model. Figure 11 represents the performance of different studied strength models taken from literature.

The ultimate loading capacity (P_O) of steel-tube CFRP confined concrete columns (STC) can be defined as:

Table 5 Statistical information of constructed database

Parameter	D (mm)	H (mm)	nt (mm)	Es (GPa)	f'_{co} (MPa)	f'_{cc} (MPa)	ε_{co} (%)	ε_{cc} (%)	$\varepsilon_{cc}/\varepsilon_{co}$	f'_{cc}/f'_{co}
Min	51	102	0.09	10	12.41	18.5	0.16	0.33	1.375	1.02
Max	406	812	5.9	612	188.2	302.2	1.53	4.62	20.76	3.9
Mean	152.9	306.2	0.85	171.3	42.27	75.73	0.27	1.59	6.59	1.95
SD	46.7	93.4	1.02	114.4	23.45	34.52	0.16	0.83	3.92	0.67
COV	0.31	0.31	1.2	0.67	0.56	0.46	0.6	0.53	0.6	0.35

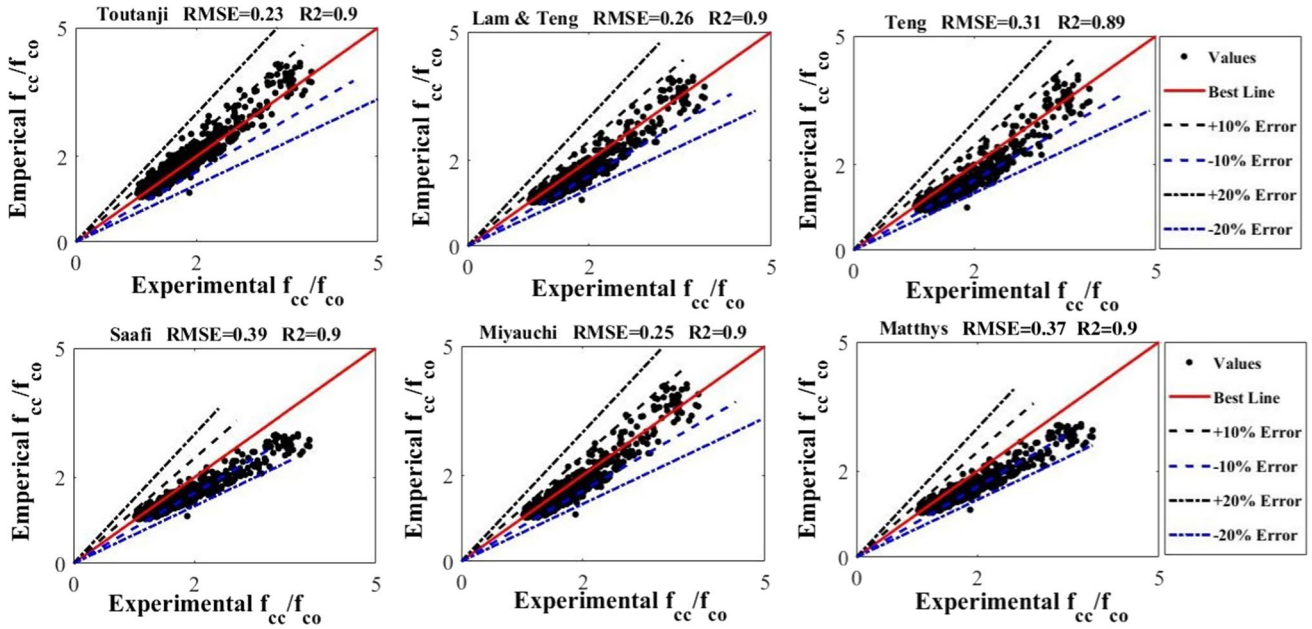

Fig. 11 Performance of previously proposed strength models of confined concrete on the developed database

$$P_{\mathrm{O}} = P_{\mathrm{conf}} + P_{\mathrm{st}} \tag{5}$$

where P_{conf} is the ultimate loading capacity of column due to confined concrete and P_{st} is the ultimate loading capacity of column due to steel tube. The ultimate loading capacity due to confinement can be expressed as:

$$P_{\mathrm{conf}} = A_{\mathrm{cc}} f'_{\mathrm{cc}} \tag{6}$$

where A_{cc} is the concrete cross-sectional core area confined by CFRPs and steel tube together and f'_{cc} is the axial strength of confined concrete. The general form of the equation of f'_{cc} was adopted from Lam and Teng model (2003) as presented in Eq. (7)

$$f'_{\mathrm{cc}} = f_{\mathrm{co}} + k f_{\mathrm{co}} \left(\frac{f_l}{f_{\mathrm{co}}} \right)^n \tag{7}$$

where f_l is maximum combined confinement stress provided by CFRP-wraps and steel tube together which can be represented by the Eq. (8) given below (Liu and Zhou 2010; Sadeghian and Fam 2015):

$$f_l = \frac{2E_{\mathrm{f}}\varepsilon_{\mathrm{h,rup}}t}{D_{\mathrm{c}}} + \frac{2t_{\mathrm{s}}f_y}{D_{\mathrm{c}} - 2t_{\mathrm{s}}} \tag{8}$$

where D_{c} is the concrete core diameter of column, E_{f} is the elastic modulus of FRPs, t_{s} is total the thickness of steel tube and $\varepsilon_{\mathrm{h,rup}}$ is the rupture strain of FRPs in hoop direction whose relation was provided by Lim et al. (2016) using genetic programming:

$$\varepsilon_{\mathrm{h,rup}} = \frac{\varepsilon_{\mathrm{f}}}{f'^{0.125}_{\mathrm{co}}} \tag{9}$$

After performing some preliminary evaluations using statistical parameters (R^2, SSE and RMSE) for the curve fitting technique in MATLAB to achieve a best fit, the selected values for the coefficients k and n were 3.07 and 0.80, respectively. Thus, the proposed analytical model for the axial strength of confined concrete was presented using Eq. (10).

$$f'_{\mathrm{cc}} = f'_{\mathrm{co}} + 3.07 f'_{\mathrm{co}} \left(\frac{f_l}{f'_{\mathrm{co}}} \right)^{0.80} \tag{10}$$

$$f'_{\mathrm{cc}} = f'_{\mathrm{co}} + 3.07 f'^{0.20}_{\mathrm{co}} f^{0.80}_l \tag{11}$$

The performance of the proposed analytical strength model for the predictions of the axial strength of confined concrete was represented in Fig. 12. It can be observed that the proposed model gave lesser error with $R^2 = 0.91$ and RMSE = 0.19 as compared with the previously proposed strength models and thus, selected in the present study.

Thus, Eq. (6) becomes as

$$P_{\mathrm{conf}} = A_{\mathrm{cc}} \left[f'_{\mathrm{co}} + 3.07 f'^{0.20}_{\mathrm{co}} f^{0.80}_l \right] \tag{12}$$

The ultimate capacity of steel tube P_{st} can be found using continuous strength method which has been established to exploit the strain hardening for determining the

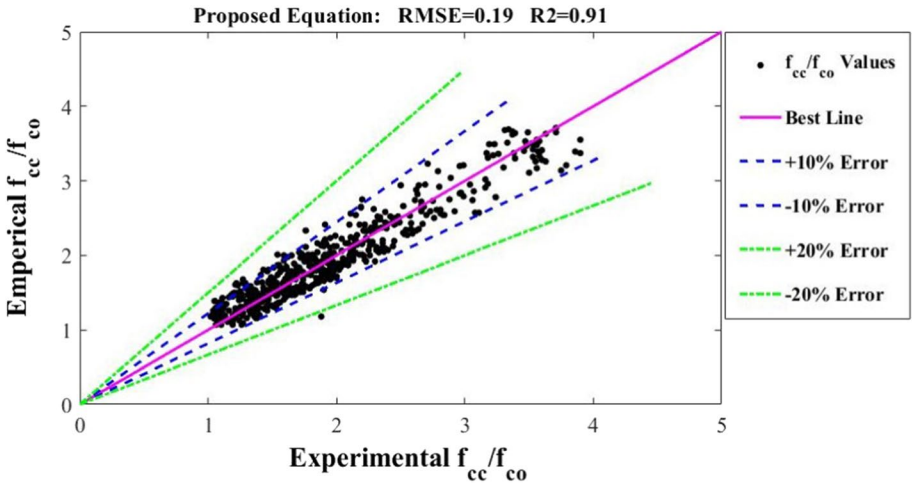

Fig. 12 Performance of proposed empirical strength model of confined concrete on the developed database

steel-tube cross section resistances (Buchanan et al. 2016; Zhao et al. 2017; Sharif et al. 2019).

$$P_{st} = A_{st}\sigma_{LB} \tag{13}$$

where A_{st} is the gross cross-sectional area of steel tube and σ_{LB} is the stress defining the local buckling of tube. Thus, the ultimate loading capacity (Po) of the STC columns can be rewritten in the following general form.

$$P_O = A_{cc}\left[f'_{co} + 3.07 f'^{0.20}_{co} f_l^{0.80}\right] + A_{st}\sigma_{LB} \tag{14}$$

This is the proposed equation predicting the maximum loading capacity of STC columns under concentric loadings. For the validation of the proposed equation, its predictions were compared with the NLFEA predictions of 216 STC columns obtained from the numerical parametric study. The theoretical results of the currently proposed equation were in close correlation with the numerical predictions with $R^2 = 0.96$ as presented in Fig. 13.

6 Conclusions

Following key points have been concluded from the presented work:

1. The dual confinement due to FRP and steel tube is the most efficient technique to enhance the loading capacity and ductility of STC columns. The FRP-confinement of CFST columns effectively prevents the outward local buckling and improves the structural performance in terms of axial loading capacity and axial deflection of STC columns. After the yielding of confining steel tube material, the impact of confinement is increased due to the incorporation of FRP material showing the column as an efficient structural member.
2. The NLFEA results demonstrated a close agreement between the experimental and the NLFEA predictions of STC columns with the average percentage discrepancies of 5.76% and 2.86% for the ultimate axial loading

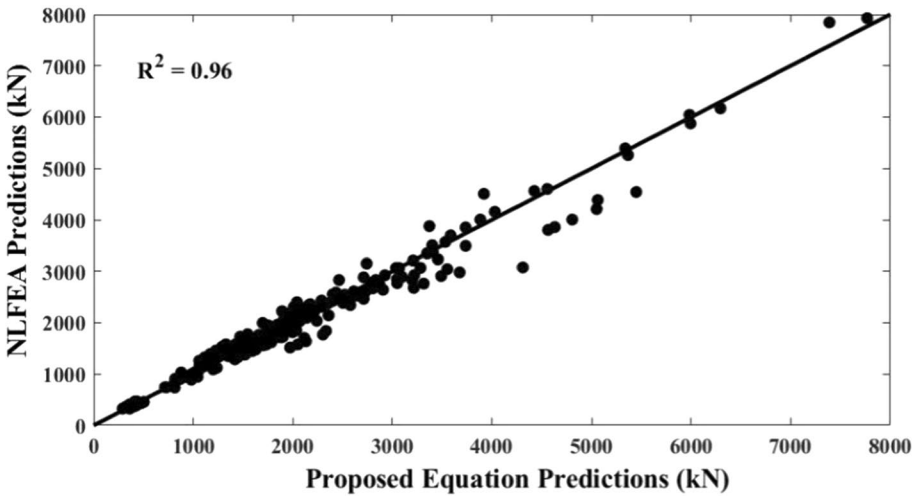

Fig. 13 Comparison between the NLFEA results and theoretical predictions of the proposed capacity equation for STC columns

capacity and corresponding axial deflection, respectively. Thus, the current finite element approach presents a helpful tool for the investigation of complex confinement mechanisms of STC columns for design purposes. The finite element crack patterns of STC columns were visualized through maximum positive principal plastic strains in ABAQUS which revealed that the experimental crack patterns were accurately traced by the NLFEA model.

3. The parametric study results revealed that with the increase of number of CFRP layers, thickness of confining steel tube, unconfined concrete axial compressive strength and diameter of columns, there was observed an increase in the axial loading capacity of STC columns. With the increase of CFRP layers from 0 to 5, the axial capacity was increased by 179.01%; with the increase of thickness of steel tube from 0.5 to 3 mm, the axial capacity was increased by 64.02%; with the increase of unconfined concrete axial strength from 15 to 65 MPa, the axial capacity was increased by 222.23% and with the increase of core diameter of concrete from 100 to 350 mm, the axial capacity was increased by 2157.44% which was the most dominant effect.
4. The proposed analytical model based on the regression analysis for predicting the ultimate axial loading capacity of STC columns presented a close agreement with the predictions of NLFEA model with a coefficient of determination of 0.96%. Thus, the proposed NLFEA model and the analytical model can be used for the analysis and design of various critical parameters of STC columns accurately.

Compliance with Ethical Standards

Conflict of interest The authors declare no conflict of interest.

References

Alfarah B, López-Almansa F, Oller S (2017) New methodology for calculating damage variables evolution in plastic damage model for RC structures. J Eng Struct 132:70–86. https://doi.org/10.1016/j.engstruct.2016.11.022

An LH, Fehling E (2016) Finite element analysis of circular steel tube confined UHPC stub columns. In: Proceedings of 1st international conference on UHPC materials and structures (UHPC 2016-China), Changsha, China, October 27–30, 2016, published by RILEM (105)

An LH, Fehling E (2017a) Analysis of circular steel tube confined UHPC stub columns. Steel Compos Struct Int J Technol 23(6):669–682

An LH, Fehling E (2017b) Numerical study of circular steel tube confined concrete (STCC) stub columns with various concrete strengths. J Constr Steel Res 136:238–255. https://doi.org/10.1016/j.jcsr.2017.05.020

An LH, Fehling E, Ismail M (2016) Numerical modelling of circular concrete filled steel tube stub columns. In: Proceedings of HiperMat 2016 4th international symposium on ultra-high-performance concrete and high-performance construction materials, Kassel, March 9–11

An LH, Ekkehard F, Binglin L, Duc-Kien T, An-Chau NV (2019) Experimental study on structural performance of UHPC and UHPFRC columns confined with steel tube. Eng Struct 187:457–477. https://doi.org/10.1016/j.engstruct.2019.02.063

Anderson TL (1995) Fracture mechanics: fundamentals and applications. CRC Press, New York

ASCE (1982) Task committee on finite element analysis of reinforced concrete structures. State-of-the-art report on finite element analysis of reinforced concrete, American Society of Civil Engineers

Ashraf M, Gardner L, Nethercot DA (2006) Finite element modelling of structural stainless-steel cross-sections. Thin Walled Struct 44(10):1048–1062. https://doi.org/10.1016/j.tws.2006.10.010

Barbero E, Cosso F, Roman R, Weadon T (2013) Determination of material parameters for Abaqus progressive damage analysis of E-glass epoxy laminates. Compos B Eng 46:211–220. https://doi.org/10.1016/j.compositesb.2012.09.069

British Standards Institution (2004) Design of concrete structures—part 1-1: general rules and rules for buildings. Eurocode 2

Buchanan C, Gardner L, Liew A (2016) The continuous strength method for the design of circular hollow sections. J Constr Steel Res 118:207–216. https://doi.org/10.1016/j.jcsr.2015.11.006

Chang X, Ru ZL, Zhou W, Zhang YB (2013) Study on concrete-filled stainless steel–carbon steel tubular (CFSCT) stub columns under compression. Thin Walled Struct 63:125–133. https://doi.org/10.1016/j.tws.2012.10.002

Chau V, An N, Le H, Thai D-K (2019) Numerical simulation and analytical assessment of STCC columns filled with UHPC and UHPFRC. Struct Eng Mech 70(1):013–31

Diaz Valdes S, Soutis C (2000) Health monitoring of composites using Lamb waves generated by piezoelectric devices. Plast Rubber Compos 29(9):496–502. https://doi.org/10.1179/146580100101541328

Díaz Valdés SH, Soutis C (2002) Real-time nondestructive evaluation of fiber composite laminates using low-frequency Lamb waves. J Acoust Soc Am 111(5):2026–2033. https://doi.org/10.1121/1.1466870

Ding FX, Liu J, Liu XM, Yu ZW, Li DW (2015) Mechanical behavior of circular and square concrete filled steel tube stub columns under local compression. Thin Walled Struct 94:155–166. https://doi.org/10.1016/j.tws.2015.04.020

Ellobody E (2013) A consistent nonlinear approach for analysing steel, cold-formed steel, stainless steel and composite columns at ambient and fire conditions. Thin Walled Struct 68:1–17. https://doi.org/10.1016/j.tws.2013.02.016

Ellobody E, Young B, Lam D (2006) Behaviour of normal and high strength concrete-filled compact steel tube circular stub columns. J Constr Steel Res 62(7):706–715. https://doi.org/10.1016/j.jcsr.2005.11.002

Fam A, Qie FS, Rizkalla S (2004) Concrete-filled steel tubes subjected to axial compression and lateral cyclic loads. J Struct Eng 130(4):631–640. https://doi.org/10.1061/(asce)0733-9445(2004)130:4(631)

Gardner L, Cruise RB, Sok CP, Krishnan K, Dos Santos JM (1900) Life-cycle costing of metallic structures. ICE, New York

Genikomsou AS, Maria Anna P (2015) Finite element analysis of punching shear of concrete slabs using damaged plasticity model

in ABAQUS. Eng Struct 98:38–48. https://doi.org/10.1016/j.engstruct.2015.04.016
Hadi MN, Khan QS, Sheikh MN (2016) Axial and flexural behavior of unreinforced and FRP bar reinforced circular concrete filled FRP tube columns. Constr Build Mater 122:43–53. https://doi.org/10.1016/j.conbuildmat.2016.06.044
Han LH, Li W, Bjorhovde R (2014) Developments and advanced applications of concrete-filled steel tubular (CFST) structures: Members. J Constr Steel Res 100:211–228. https://doi.org/10.1016/j.jcsr.2014.04.016
Hany NF, Hantouche EG, Harajli MH (2016) Finite element modeling of FRP-confined concrete using modified concrete damaged plasticity. Eng Struct 125:1–14. https://doi.org/10.1016/j.engstruct.2016.06.047
Hashin Z (1980) Failure criteria for unidirectional fiber composites. J Appl Mech 47(2):329–334. https://doi.org/10.1115/1.3157744
Hashin Z, Rotem A (1973) A fatigue failure criterion for fiber reinforced materials. J Compos Mater 7(4):448–464. https://doi.org/10.1177/002199837300700404
Hassanein M (2010) Numerical modelling of concrete-filled lean duplex slender stainless-steel tubular stub columns. J Constr Steel Res 66(8–9):1057–1068. https://doi.org/10.1016/j.jcsr.2010.03.008
Hassanein M, Kharoob O, Liang Q (2013) Behaviour of circular concrete-filled lean duplex stainless steel–carbon steel tubular short columns. Eng Struct 56:83–94. https://doi.org/10.1016/j.engstruct.2013.04.016
Hoang AL, Fehlinga E (2017) Numerical analysis of circular steel tube confined UHPC stub columns. Comput Concr 19(3):263–273. https://doi.org/10.12989/cac.2017.19.3.263
Hoang AL, Fehling E, Thai DK, Nguyen CV (2019) Evaluation of axial strength in circular STCC columns using UHPC and UHPFRC. J Constr Steel Res 153:533–549
Hu HT, Huang CS, Wu MH, Wu YM (2003) Nonlinear analysis of axially loaded concrete-filled tube columns with confinement effect. J Struct Eng 129(10):1322–1329. https://doi.org/10.1061/(asce)0733-9445(2003)129:10(1322)
Hu B, Wang JG, Li GQ (2011) Numerical simulation and strength models of FRP-wrapped reinforced concrete columns under eccentric loading. Constr Build Mater 25(5):2751–2763. https://doi.org/10.1016/j.conbuildmat.2010.12.036
Huang L, Zhang S, Yu T, Wang Z (2018) Compressive behaviour of large rupture strain FRP-confined concrete-encased steel columns. Constr Build Mater 183:513–522. https://doi.org/10.1016/j.conbuildmat.2018.06.074
Jiang T, Teng J (2007) Analysis-oriented stress–strain models for FRP—confined concrete. Eng Struct 29(11):2968–2986. https://doi.org/10.1016/j.engstruct.2007.01.010
Kachlakev DI, Miller TH, Potisuk T, Yim SC, Chansawat K (2001) Finite element modeling of reinforced concrete structures strengthened with FRP laminates, Oregon. Department of Transportation. Research Group, New York
Karabinis A, Rousakis T (2002) Concrete confined by FRP material: a plasticity approach. Eng Struct 24(7):923–932. https://doi.org/10.1016/s0141-0296(02)00011-1
Lam D, Gardner L (2008) Structural design of stainless-steel concrete filled columns. J Constr Steel Res 64(11):1275–1282. https://doi.org/10.1016/j.jcsr.2008.04.012
Lam L, Teng J (2003) Design-oriented stress–strain model for FRP-confined concrete. Constr Build Mater 17(6–7):471–489
Le AH, Ekkehard F, Thai DK, Nguyen CV (2018) Simplified stress–strain model for circular steel tube confined UHPC and UHPFRC columns. Steel Compos Struct 29(1):125–138
Lee J, Fenves GL (1998) A plastic-damage concrete model for earthquake analysis of dams. Earthq Eng Struct Dyn 27(9):937–956. https://doi.org/10.1002/eqe.2317
Liew JR, Xiong D (2009) Effect of preload on the axial capacity of concrete-filled composite columns. J Constr Steel Res 65(3):709–722. https://doi.org/10.1016/j.jcsr.2008.03.023
Lim JC, Karakus M, Ozbakkaloglu T (2016) Evaluation of ultimate conditions of FRP-confined concrete columns using genetic programming. Comput Struct 162:28–37. https://doi.org/10.1016/j.compstruc.2015.09.005
Liu J, Zhou X (2010) Behavior and strength of tubed RC stub columns under axial compression. J Constr Steel Res 66(1):28–36. https://doi.org/10.1016/j.jcsr.2009.08.006
Liu JP, Xu TX, Wang YH, Guo Y (2018) Axial behaviour of circular steel tubed concrete stub columns confined by CFRP materials. Constr Build Mater 168:221–231. https://doi.org/10.1016/j.conbuildmat.2018.02.131
Majewski S (2003) The mechanics of structural concrete in terms of elasto-plasticity. Publishing House of Silesian University of Technology, Gliwice
Mander JB, Priestley MJ, Park R (1988) Theoretical stress–strain model for confined concrete. J Struct Eng 114(8):1804–1826
Matthews FL, Davies G, Hitchings D, Soutis C (2000) Finite element modelling of composite materials and structures. Elsevier, Berlin
Matthys S, Toutanji H, Audenaert K, Taerwe L (2005) Axial load behavior of large-scale columns confined with fiber-reinforced polymer composites. ACI Struct J 102(2):258. https://doi.org/10.14359/14277
Mazzucco G, Salomoni VA, Majorana CE, Pellegrino C, Ceccato C (2016) Numerical investigation of concrete columns with external FRP jackets subjected to axial loads. Constr Build Mater 111:590–599. https://doi.org/10.1016/j.conbuildmat.2016.02.050
Miyauchi K (1997) Estimation of strengthening effects with carbon fiber sheet for concrete column. In: Proceedings of the 3rd international symposium on non-metallic (FRP) reinforcement for concrete structures. Japan Concrete Institute
Najafgholipour MA, Dehghan SM, Dooshabi A, Niroomandi A (2017) Finite element analysis of reinforced concrete beam–column connections with governing joint shear failure mode. Latin Am J Solids Struct 14(7):1200–1225. https://doi.org/10.1590/1679-78253682
Nayal R, Rasheed HA (2006) Tension stiffening model for concrete beams reinforced with steel and FRP bars. J Mater Civ Eng 18(6):831–841. https://doi.org/10.1061/(asce)0899-1561(2006)18:6(831)
O'Shea MD, Bridge RQ (2000) Design of circular thin-walled concrete filled steel tubes. J Struct Eng 126(11):1295–1303
Patel VI, Hassanein MF, Thai HT, Al Abadi H, Paton-Cole V (2017) Behaviour of axially loaded circular concrete-filled bimetallic stainless-carbon steel tubular short columns. Eng Struct 147:583–597. https://doi.org/10.1016/j.engstruct.2017.05.064
Patel VI, Liang QQ, Hadi MN (2014) Nonlinear analysis of axially loaded circular concrete-filled stainless steel tubular short columns. J Constr Steel Res 101:9–18. https://doi.org/10.1016/j.jcsr.2014.04.036
Perea T, Leon RT, Hajjar JF, Denavit MD (2014) Full-scale tests of slender concrete-filled tubes: Interaction behavior. J Struct Eng 140(9):04014054. https://doi.org/10.1061/(asce)st.1943-541x.0000949
Piscesa B, Attard MM, Samani AK (2017) Three-dimensional finite element analysis of circular reinforced concrete column confined with FRP using plasticity model. J Proc Eng 171:847–856. https://doi.org/10.1016/j.proeng.2017.01.377
Rasmussen KJ, Burns T, Bezkorovainy P, Bambach MR (2003) Numerical modelling of stainless steel plates in compression. J Constr Steel Res 59(11):1345–1362. https://doi.org/10.1016/s0143-974x(03)00086-5
Raza A, Khan QUZ (2020) Experimental and numerical behavior of hybrid fiber reinforced concrete compression members under

concentric loading. SN Appl Sci. https://doi.org/10.1007/s42452-020-2461-5

Raza A, Khan QUZ, Ahmad A (2019) Numerical investigation of load-carrying capacity of GFRP-reinforced rectangular concrete members using CDP model in ABAQUS. Adv Civ Eng 2019:21. https://doi.org/10.1155/2019/1745341

Raza A, Shah SAR, Khan AR, Aslam MA, Khan TA, Arshad K, Hussan S, Sultan A, Shahzadi G, Waseem M (2020) Sustainable FRP-confined symmetric concrete structures: an application experimental and numerical validation process for reference data. Appl Sci 10(1):333. https://doi.org/10.3390/app10010333

Richart FE, Brandtzaeg A, Brown RL (1928) A study of the failure of concrete under combined compressive stresses. University of Illinois at Urbana Champaign, College of Engineering, New York

Rousakis TC, Karabinis AI, Kiousis PD, Tepfers R (2008) Analytical modelling of plastic behaviour of uniformly FRP confined concrete members. Compos B Eng 39(7–8):1104–1113. https://doi.org/10.1016/j.compositesb.2008.05.001

Saafi M, Toutanji HA, Li Z (1999) Behavior of concrete columns confined with fiber reinforced polymer tubes. ACI Mater J 96(4):500–509. https://doi.org/10.14359/652

Sadeghian P, Fam A (2015) Improved design-oriented confinement models for FRP-wrapped concrete cylinders based on statistical analyses. Eng Struct 87:162–182. https://doi.org/10.1016/j.engstruct.2015.01.024

Sharif AM, Al-Mekhlafi GM, Al-Osta MA (2019) Structural performance of CFRP-strengthened concrete-filled stainless-steel tubular short columns. Eng Struct 183:94–109. https://doi.org/10.1016/j.engstruct.2019.01.011

Shi Y, Swait T, Soutis C (2012) Modelling damage evolution in composite laminates subjected to low velocity impact. J Compos Struct 94(9):2902–2913. https://doi.org/10.1016/j.compstruct.2012.03.039

Tam VW, Wang ZB, Tao Z (2014) Behaviour of recycled aggregate concrete filled stainless steel stub columns. Mater Struct 47(1–2):293–310. https://doi.org/10.1617/s11527-013-0061-1

Tao Z, Uy B, Liao FY, Han LH (2011) Nonlinear analysis of concrete-filled square stainless-steel stub columns under axial compression. J Constr Steel Res 67(11):1719–1732

Tao Z, Wang ZB, Yu Q (2013) Finite element modelling of concrete-filled steel stub columns under axial compression. J Constr Steel Res 89:121–131. https://doi.org/10.1016/j.jcsr.2013.07.001

Teng J, Jiang T, Lam L, Luo Y (2009) Refinement of a design-oriented stress–strain model for FRP-confined concrete. J Compos Constr 13(4):269–278. https://doi.org/10.1061/(asce)cc.1943-5614.0000012

Teng J, Xiao Q, Yu T, Lam L (2015) Three-dimensional finite element analysis of reinforced concrete columns with FRP and/or steel confinement. Eng Struct 97:15–28. https://doi.org/10.1016/j.engstruct.2015.03.030

Theofanous M, Chan TM, Gardner L (2009) Structural response of stainless steel oval hollow section compression members. Eng Struct 31(4):922–934. https://doi.org/10.1016/j.engstruct.2008.12.002

Toutanji HA (1999) Stress–strain characteristics of concrete columns externally confined with advanced fiber composite sheets. ACI Mater J 96(3):397–404. https://doi.org/10.14359/639

Van Den Einde L, Zhao L, Seible F (2003) Use of FRP composites in civil structural applications. J Constr Build Mater 17(6–7):389–403

Voyiadjis GZ, Taqieddin ZN (2009) Elastic plastic and damage model for concrete materials: part I—theoretical formulation. Int J Struct Changes Solids 1(1):31–59

Wahalathantri BL, Thambiratnam DP, Chan THT, Fawzia S (2011) A material model for flexural crack simulation in reinforced concrete elements using ABAQUS. In: Proceedings of the first international conference on engineering, designing and developing the built environment for sustainable wellbeing. Queensland University of Technology

Wang YB, Liew JR (2016) Constitutive model for confined ultra-high strength concrete in steel tube. Constr Build Mater 126:812–822. https://doi.org/10.1016/j.conbuildmat.2016.09.079

Wu JY, Li J, Faria R (2006) An energy release rate-based plastic-damage model for concrete. Int J Solids Struct 43(3–4):583–612. https://doi.org/10.1016/j.ijsolstr.2005.05.038

Xiao Y (2004) Applications of FRP composites in concrete columns. Adv Struct Eng 7(4):335–343. https://doi.org/10.1260/1369433041653552

Xiong MX, Xiong DX, Liew JR (2017) Axial performance of short concrete filled steel tubes with high-and ultra-high-strength materials. Eng Struct 136:494–510. https://doi.org/10.1016/j.engstruct.2017.01.037

Youssf O, ElGawady MA, Mills JE, Ma X (2014) Finite element modelling and dilation of FRP-confined concrete columns. Eng Struct 79:70–85. https://doi.org/10.1016/j.engstruct.2014.07.045

Yu T, Teng J, Wong Y, Dong S (2010a) Finite element modeling of confined concrete-I: Drucker-Prager type plasticity model. Eng Struct 32(3):665–679. https://doi.org/10.1016/j.engstruct.2009.11.014

Yu T, Teng JG, Wong YL, Dong SL (2010b) Finite element modeling of confined concrete-II: plastic-damage model. Eng Struct 32(3):680–691. https://doi.org/10.1016/j.engstruct.2009.11.013

Zhao O, Afshan S, Gardner L (2017) Structural response and continuous strength method design of slender stainless-steel cross-sections. Eng Struct 140:14–25. https://doi.org/10.1016/j.engstruct.2017.02.044